Available online at www.sciencedirect.com
SCIENCE DIRECT®
Radiation Measurements 39 (2005) 263–275
Radiation Measurements
www.elsevier.com/locate/radmeas

Evaluation of ZnS:Cu phosphor as X-ray to light converter under mammographic conditions

I. Kandarakis[a,*], D. Cavouras[a], D. Nikolopoulos[a], A. Anastasiou[a], N. Dimitropoulos[b], N. Kalivas[c], E. Ventouras[a], I. Kalatzis[a], C. Nomicos[d], G. Panayiotakis[c]

[a] *Department of Medical Instruments Technology, Technological Educational Institution of Athens, Agiou Spyridonos, Egaleo, 122 10 Athens, Greece*
[b] *Department of Medical Imaging, "Euromedica" Medical Center, 2 Mesogeion Avenue, Athens, Greece*
[c] *Department of Medical Physics, Medical School, University of Patras, 265 00 Patras, Greece*
[d] *Department of Electronics, Technological Educational Institution of Athens, Agiou Spyridonos Street, Egaleo, 122 10 Athens, Greece*

Received 10 November 2003; received in revised form 30 January 2004; accepted 14 February 2004

Abstract

The aim of the present study was to evaluate ZnS:Cu phosphor for use in X-ray mammographic detectors. This phosphor has never been used in medical imaging probably due to its moderate scintillation decay time. However, it may be suitable for non-dynamic medical imaging, due to its "green" emission spectrum, which is compatible with the sensitivity of many currently used photodetectors, and its high X-ray to light intrinsic conversion efficiency. ZnS:Cu phosphor powder was used to prepare several test screens in laboratory. Parameters related to light emission and image quality properties were experimentally as well as theoretically evaluated and compared to those of other known ZnS-based phosphor materials. Results showed that ZnS:Cu performed adequately well in the mammographic energy range.

Keywords: Phosphor screens; Luminescence efficiency; Image quality

1. Introduction

The performance of phosphor materials, or scintillators, incorporated in medical imaging detectors, is determined by the X-ray absorption efficiency, the light emission characteristics and the compatibility of the phosphor's light spectrum to the spectral sensitivity of photodetectors (films, photodiode arrays, CCDs, photocathodes) (Hell et al., 2000; Wieczorek, 2001; van Eijk, 2002).

Zinc sulfide (ZnS)-based phosphor materials have been reported to be of very high intrinsic conversion efficiency, i.e. conversion of X-rays into light (Alig and Bloom, 1977). In addition, the density of ZnS (4.09 g/cm^3) could be considered adequate for radiation detection, being higher than that of many currently used phosphors or scintillators such as NaI. Silver-activated zinc sulfide (ZnS:Ag) has been previously used in nuclear radiation detection instruments (Knoll, 1989). Due to their low effective atomic number, ZnS phosphors could only be suitable for use with low energy X-rays, which, however, are employed in many radiographic examinations. The use of ZnS:Ag in X-ray imaging detectors is limited by its low wavelength emission spectrum (450 nm). The latter exhibits poor spectral compatibility with many photodetectors currently employed in medical imaging. Additionally, the high-frequency bluish ZnS:Ag light is expected to show significant attenuation within the phosphor material, since light attenuation increases with frequency (van de Hulst, 1957). When zinc sulfide phosphor is activated with copper (ZnS:Cu), green light emission is induced. This light is within the limits of the spectral sensitivities of currently used photodetectors, designed to match the spectra of green emitting rare earth phosphors. To our knowledge, ZnS:Cu has never been previously used or

* Corresponding author. Tel.: +3010-5385-375; fax: +3010-5910-975.
E-mail address: kandarakis@teiath.gr (I. Kandarakis).

1350-4487/$ - see front matter © 2004 Elsevier Ltd. All rights reserved.
doi:10.1016/j.radmeas.2004.02.023

studied as X-ray to light converter in medical imaging. It has only been employed as electron to light converter in the output screens of image intensifiers and of screens in display units (van Eijk, 2002).

Although ZnS:Cu phosphor has relatively low effective atomic number, it may be suitable for mammography. This is because the energy of the photoelectric K-absorption edge of zinc, lying at 9.6 keV, results in increased X-ray absorption in the low-energy range employed in mammography. On the other hand, the K-characteristic X-ray fluorescence yield, which reduces light output and image quality, is low (0.479). The corresponding value for Gd, mostly employed in rare earth radiography screens, is 0.934 (Hubbell et al., 1994), while the Gd K-absorption energy is at 50.2 keV. Additionally, the ZnS energy gap, separating the valence and conduction energy bands is very low (3.8 eV) (Alig and Bloom, 1977; Blasse, 1994). Thus, relatively low energy is required to raise an electron from the valence to the conduction band and to produce molecular excitations and light emission. As a result, the intrinsic efficiency for conversion of the absorbed X-ray energy into light is expected to be very high (Alig and Bloom, 1977). The main disadvantage of ZnS:Cu seems to be its moderate scintillation decay time. This, however, is not a problem for mammography, either conventional or digital, since only static imaging is performed for breast cancer diagnosis.

The aim of the present study was to examine the suitability of ZnS:Cu for X-ray mammographic imaging and compare it to other ZnS-based phosphors, namely, ZnS:Ag, ZnSCdS:Ag, and ZnSCdS:Cu,Au. ZnS:Cu was used in the form of granular screens of various thicknesses, prepared from powder grains, similar to those typically employed in X-ray medical imaging. The following parameters were determined (Ludwig, 1971; Dick and Motz, 1981; Blasse, 1994; Kandarakis et al., 1997; 2001a–c):

1. The absolute luminescence efficiency (AE), expressing the emission efficiency of a phosphor material and defined in terms of the emitted light energy flux per unit of incident X-ray exposure. AE was both experimentally and theoretically evaluated.
2. The modulation transfer function (MTF), describing the variation of contrast with spatial frequency and hence expressing spatial resolution. MTF was both experimentally and theoretically evaluated.
3. The detective quantum efficiency (DQE), expressing the degradation of the signal-to-noise ratio (SNR) of a real imaging system with respect to that of an ideal system.
4. The phosphor's emission spectrum, which was experimentally determined and it was used to evaluate the spectral compatibility of ZnS:Cu to various photodetectors.
5. Finally, the intrinsic conversion efficiency, expressing the fraction of absorbed X-ray energy converted into light within the mass of the phosphor, and the light attenuation properties (scattering and absorption) of the ZnS:Cu phosphor were examined.

2. Materials and methods

2.1. Theory

The output signal of an X-ray-irradiated phosphor is expressed via the emitted light energy flux (emitted light energy per unit of area and time), $\bar{\Psi}_\lambda$, given as follows:

$$\bar{\Psi}_\lambda(E_O, w_O) = \int_0^{E_O} \bar{\Psi}_X(E)\bar{\eta}_\varepsilon(E, w_O)\eta_C(\lambda) \times \int_0^{w_O} \psi(E, w)\bar{g}_\lambda(\sigma, w)\,dw\,dE, \quad (1)$$

where $\bar{\Psi}_X$ denotes the incident X-ray energy flux, E_O is the maximum energy of the spectrum of X-rays determined by the tube high voltage, w_O is the thickness (or coating weight) of the phosphor being in the form of a phosphor screen (fluorescent layer), E is the energy of an X-ray photon, η_ε is the energy absorption efficiency being the fraction of incident X-ray energy flux absorbed by the phosphor. The absorption efficiency is an exponential function of the X-ray energy absorption coefficient (Hubbell and Seltzer, 1995). η_C is the intrinsic X-ray to light conversion efficiency, which expresses the fraction of absorbed X-ray energy that is converted into light within the phosphor material. ψ is a function giving the probability of an absorbed X-ray photon of energy E to be absorbed at a depth $w < w_O$. g_λ is the fraction of light energy, created at depth w, that escapes the phosphor following the absorption of one X-ray photon. σ is an optical attenuation coefficient accounting for the attenuation of light within the phosphor (Ludwig, 1971; Swank, 1973). The second integral in (1) describes the light attenuation within the phosphor layer and defines the light transmission efficiency of the phosphor (Hamaker, 1947; Ludwig, 1971; Swank, 1973; Kandarakis et al., 1997, 2001a–c). Scattering of light is the main light attenuation mechanism since the phosphor is in the form of grains, which act as light scatterers. Another minor factor of light losses is due to light absorption. The first integral is applied to integrate over the energies of the X-ray spectrum. Mean values in (1) express averaging of the corresponding parameters over the area of the detector.

The absolute luminescence efficiency (η_A) of a phosphor is defined by the relation (Ludwig, 1971; Kandarakis et al., 1997):

$$\eta_A(E_O, w_O) = \frac{\bar{\Psi}_\lambda(E_O, w_O)}{\dot{X}(E_O)}, \quad (2)$$

where $\dot{X}$ is the exposure rate incident on the phosphor.

To express the compatibility of emitted light energy flux with the spectral sensitivity of the photodetector, the spectral matching factor f_S, was calculated by the relation (Kandarakis et al., 1997, 2001b)

$$f_S = \int_{\lambda_1}^{\lambda_2} \varepsilon_P(\lambda)S_{OD}(\lambda)\,d\lambda \Big/ \int_{\lambda_2}^{\lambda_1} S_{OD}(\lambda)\,d\lambda, \quad (3)$$

where $\varepsilon_P(\lambda)$ is the spectrum of the light emitted by the phosphor and $S_{OD}(\lambda)$ is the spectral sensitivity of the photodetector combined with the phosphor. λ denotes light photon wavelength.

Most parameters describing image quality have been traditionally defined in terms of the emitted light photon flux (i.e. number of light photons per unit of area and time) (Shaw and Van Metter, 1984). The latter may be expressed as follows:

$$\bar{\Phi}_\lambda(E_O, w) = \int_0^{E_O} \bar{\Phi}_X(E)\bar{\eta}_\varepsilon(E, w)\bar{m}_O(E, \lambda) \times \int_0^{w_0} \psi(E, w)\bar{g}_\lambda(\sigma, w)\, dw\, dE, \quad (4)$$

where $\bar{\Phi}_\lambda$ denotes the emitted light photon flux, in photons per unit of screen area, averaged over the screen surface. $\bar{\Phi}_X$ is the incident X-ray photon flux, in photons per unit of screen area, averaged over the screen surface. $\bar{m}_O$ is the number of light photons generated within the phosphor material per X-ray photon absorbed (Shaw and Van Metter, 1984).

Relation (4) may be Fourier transformed and may be expressed in the spatial frequency domain as a function of spatial frequency u (see Appendix A). Using the frequency-dependent light photon flux, the MTF M and the gain transfer function G, may be defined, as follows:

$$M(u, w_O) = \frac{\bar{\Phi}_\lambda(u, w_O)}{\bar{\Phi}_\lambda(0, w_O)}, \quad (5)$$

$$G(u, w_O) = \frac{\bar{\Phi}_\lambda(u, w_O)}{\bar{\Phi}_X(E_O)}, \quad (6)$$

where the denominator in Eq. (6) represents the incident X-ray photon flux integrated over the X-ray spectrum. $M$is the spatial frequency-dependent light photon flux normalized to the zero frequency light flux. For zero spatial frequency ($u=0$), $M=1$. For the same frequency, G equals the mean number of emitted light photons per incident X-ray, under uniform screen irradiation. Thus G ($u=0$) may be defined as the detector's optical gain G_D, expressing the net photon amplification in a phosphor screen.

Using Eqs. (5) and (6) and G_D definition, G may be written:

$$G(u, w_O) = \frac{\bar{\Phi}_\lambda(0, w_O)\bar{\Phi}_\lambda(u, w_O)}{\bar{\Phi}_X(E_O)\bar{\Phi}_\lambda(0, w_O)} = G_D(w_O)M(u, w_O). \quad (7)$$

Then the output signal of a phosphor screen may be expressed as follows:

$$\bar{\Phi}_\lambda(u, w_O) = \bar{\Phi}_X(E_O)G_D(w_O)M(u, w_O). \quad (8)$$

Of primary importance in X-ray imaging detectors is to improve the SNR. SNR is usually expressed via the DQE, which is defined by the equation (Dick and Motz, 1981; Shaw and Van Metter, 1984):

$$DQE(u, w) = \frac{[SNR_O(u, w)]^2}{[SNR_I]^2}. \quad (9)$$

SNR_O is the output SNR while SNR_I is the input SNR or the SNR of an ideal imaging system. The numerator in (9) may be written:

$$SNR_O^2(u, w_O) = \frac{\bar{\Phi}_\lambda^2(u, w_O)}{N_Q^2(u, w_O)} = \frac{[\bar{\Phi}_X(E_O)G_D(w_O)M(u, w_O)]^2}{W_Q(u, w_O)}, \quad (10)$$

where N_Q is the noise amplitude spectrum and W_Q is the noise power spectrum (NPS), or Wiener spectrum (Shaw and Van Metter, 1984). The latter equals the noise amplitude squared. NPS is given as the Fourier transform of the light photon flux fluctuations when a phosphor screen is uniformly irradiated. These fluctuations are expressed by the statistical variance in the light photon flux values. Thus NPS may be expressed in terms of the functions $\eta_\varepsilon, m_O, g_\lambda$ used previously in the definition of light photon flux (Eq. (4)) (Shaw and Van Metter, 1984).

SNR_I squared, in Eq. (9), may be expressed in terms of the square of the mean incident X-ray energy flux. (Shaw and Van Metter, 1984; Williams et al., 1999). However, calculations using X-ray spectrum (Williams et al., 1999), have shown that photon flux may be used with no significant loss (lower than 4 %) of experimental accuracy. Since X-ray photons follow Poisson statistics, SNR_I squared may be considered approximately equal to the incident X-ray photon flux $\bar{\Phi}_X(E_O)$ (Williams et al., 1999). Thus DQE may be written as follows:

$$DQE(u, w_O) = \frac{\bar{\Phi}_X(E_O)[G_D(w_O)M(u, w_O)]^2}{W_Q(u, w_O)}. \quad (11)$$

2.2. Experiments

ZnS:Cu was purchased in powder form (Derby Luminescents Ltd, UK) with mean grain size of approximately 7 μm. The phosphor was used in the form of thin layers (test screens) to simulate the intensifying screens employed in X-ray radiography. Several screens with coating thicknesses of approximately 20, 43, 70, 100, 150 mg/cm^{2}were prepared in our laboratory by sedimentation of the powder on fused silica substrates (spectrosil B). During the sedimentation process, sodium orthosilicate (Na_2SiO_3) was used as binding material between the powder grains (Kandarakis et al., 2001b).

The absolute efficiency was determined by light energy flux and incident exposure rate measurements (see relation (2)), which are described below. The detector optical gain was determined by converting light energy flux into light photon flux and exposure rate into X-ray photon flux (see below) as required by relations (4) and (6).

The phosphor screens were exposed to X-rays on a General Electric DMR Plus mammographic unit, employing X-ray tube voltages ranging from 22 to 40 kVp with molybdenum/molybdenum (Mo/Mo) anode/filter combination and 650 mm focus to film distance (FFD). To simulate

X-ray attenuation and spectrum shape alteration by human breast, the beam was transmitted through a 3.5 cm thick slab of Lucite. The light energy flux was measured, during X-ray exposure of the screens, using a photomultiplier (EMI 9558 QB) coupled to an electrometer (Cary 401). The photomultiplier was operated as a simple photocathode to avoid photocurrent instability. The light photon flux was determined after division of Ψ_λ values by the mean light photon energy. The latter was determined by light emission spectrum measurements (performed with an Oriel 7240 monochromator). Two modes of light flux measurements were followed: (1) Reflection mode, where light emitted by irradiated screen side was measured. (2) Transmission mode where the non-irradiated screen side's light was measured. Reflection mode represents the conventional mammography intensifying screens and the rear screens of an ordinary radiographic cassette. Transmission mode simulates all the other X-ray-imaging modalities (digital detectors, image intensifiers, front screens of radiographic cassettes, computed tomography detectors). In both cases light flux data were corrected by taking into account light losses due to (1) the geometric light collection efficiency (GCE) of the experimental set-up and (2) the light spectral mismatches between the screen light and the photocathode sensitivity (extended S/20). GCE depends on (a) the distance between the screen and the photocathode of the photomultiplier and (b) the angular distribution of emitted light. The latter was experimentally determined by a photomultiplier performing an angular translation obtained via step-scan controller associated with a Rigaku–Denki (SG-9D type) horizontal goniometer rotating within a 180° angle with a step accuracy of 0.05°. Spectral mismatches were corrected by dividing light flux data by the corresponding spectral compatibility factor (see Eq. (3)).

X-ray exposure was measured by an ionization chamber dosimeter (RTI, Solidose R100). Exposure data were converted into X-ray photon flux using the corresponding conversion factor (Greening, 1985):

$$\dot{\Psi}_X/\dot{X} = [\bar{W}_a/e](\mu_{en}(E)/\rho)^{-1}_{air} \quad (12)$$

with $\bar{W}_a$ being the mean energy required to create an electron ion pair in air and $(\mu_{en}/\rho)_{air}$ is the mass energy absorption coefficient for air. Photon flux may be converted into X-ray energy flux by multiplying with the photon energy E. Since polyenergetic beams are employed in X-ray imaging, mean X-ray energy $\bar{E}$ (E averaged over the X-ray spectrum) and the corresponding $\mu_{en}(\bar{E})$ were used in relation (12).

The emitted light spectrum, $\varepsilon_P(\lambda)$ in relation (3), was measured by an Oriel 7240 grating monochromator while the spectral sensitivities $S_{OD}(\lambda)$ of the photodetectors (relation (3)) were obtained from the manufacturers' data.

MTF was determined by the square-wave response function (SWRF) method (Barnes, 1979; ICRU, 1986). An MTF test pattern (typ-53, Nuclear Associates), with lead lines of various widths corresponding to spatial frequencies from 0.25 to 10 lp/mm was used. Agfa mamoray HD-S radiographic film was used to obtain pattern images. In reflection mode measurements the film was placed behind the test pattern and in front of the screen. In transmission mode the film was placed behind the screen. The pattern-film–screen system, corresponding to each screen, was exposed to X-rays under conditions identical to those employed for light flux measurements. The films were then developed to obtain the pattern images, as optical density variations, which by definition are the SWRFs (Barnes, 1979; ICRU, 1986). The film processor was an Agfa mamoray operated at temperature of 36°C and at 90 s processing time. Then the film images were digitized on a Microtec Scanmaker II SP (1200 × 1200 dpi). The MTFs were finally calculated from the digitized image optical density variations (digital SWRF) across directions vertical with respect to the images of the test pattern lines, employing Coltman's formula (Barnes, 1979; ICRU, 1986). The latter gives the MTF as a function of SWRF. The MTF data, obtained in this way, were corrected by dividing by the MTF of the scanner and the MTF of the film, both measured in a previous study (Kandarakis et al., 2001c).

NPS was determined following the typical auto-correlation function technique described in detail in previous studies (Williams et al., 1999; Kandarakis et al., 2001c). Uniform irradiation of the ZnS:Cu screen–film combinations was performed employing the same exposure conditions as those for absolute efficiency and MTF measurements. No test pattern was used. Both reflection and transmission NPS measurements were followed. The NSP was obtained by Fourier transforming the auto-correlation function, expressing the importance of the optical density fluctuations obtained on the film after irradiation. Film images were digitized as in the case of MTF determination.

Frequency-dependent DQE was determined by relation (11) using X-ray photon flux, detector gain, MTF and NPS data.

2.3. Calculations

Using relations (1), (2), (4)–(6), (11) in combination with (A.1) and (A.2) in Appendix A, the absolute efficiency, the MTF, the gain transfer function, the NPS and the DQE may be also calculated as functions of the intrinsic physical parameters of the phosphor material. The corresponding theoretical expression for absolute efficiency (relations (1), (2), (A.1), and (A.2)) was used to fit experimental absolute efficiency data. Fitting was performed by the Levenberg–Marquard method (Press et al., 1990) using the optical attenuation coefficients σ and β_0 (see relation (A.2)) as fitting parameters. The physical quantities contained in relations (1) and (4) may be expressed by the following functions:

The incident X-ray energy flux $\bar{\Psi}_X(E)$ and the incident light photon flux $\bar{\Phi}_X(E)$ were expressed and calculated using the appropriate conversion factor (relation (12)) and the theoretical model (Tucker et al., 1991) approximating the energy spectral distribution of the X-rays produced by a

molybdenum or tungsten target X-ray tube. This model was employed to express X-ray energy flux in (1), (2), and X-ray photon flux, in relations (4)–(11).

The energy absorption efficiency η_ε, in relations (1) and (4), was calculated by considering exponential X-ray absorption within the phosphor material. Exponential formulas were expressed in terms of the X-ray total mass energy absorption coefficient (μ_{en}/ρ) and the thickness w of the phosphor layer. The X-ray energy absorption coefficient of ZnS was calculated using the corresponding coefficients of Zn and S obtained from published data (Storm and Israel, 1967; Hubbell and Seltzer, 1995).

In addition to absorption and detection efficiency calculations the interaction of X-ray photons within ZnS phosphor was examined by a custom developed software for Monte-Carlo simulation. This software was developed and applied to investigate the transport of photons through phosphor screens as a function of X-ray energy and screen thickness. The three basic interaction processes, which govern this transport, i.e. photoelectric absorption, coherent and incoherent scattering were taken into consideration. The code was based on the generation of random numbers, which were considered to represent random photon events. According to this random event simulation, photon track and energy histories were recorded, thus yielding the determination of the energy transferred to the medium. The code was fed with the interaction cross-sectional data and the non-relativistic form and scatter factors of ZnS phosphor investigated. The data were downloaded from NIST Reference Database [http://physics.nist.gov/PhysRefData/]. The general scheme of the code used in this study was as follows: a photon of energy E is incident normally at the center of the top surface of a screen of known dimensions. Using random numbers and the cross-sectional data, the interaction type and site were determined. In the case of scatter events, the following parameters were determined: (i) site and type of subsequent interaction, (ii) energy of X-ray photon after the interaction and (iii) energy transferred to the medium. This was achieved by taking into account the cross-sectional, form factor and scatter factor data (Hubbell et al., 1975; Hubbell and Overbo, 1979) and by following methods described in previous studies (Chan and Doi, 1983). The process was continued until the photon escaped the screen or it was absorbed within the phosphor material. In the latter case, the photon energy E minus the energy corresponding to the photoelectric K-absorption edge of zinc (9.6 keV), was considered to be transferred to the medium. All photon track and energy histories were stored for further processing. To validate our Monte-Carlo code, data for the well-known Gd_2O_2S phosphor were also derived. These data were compared and found close to data already published by others (Boone et al., 1999).

The X-ray energy into light conversion efficiency of the phosphor material, η_C in relation (1), and the number of light photons generated within the phosphor per absorbed X-ray, $\bar{m}_O$ in relation (4), may be calculated by the relations (Alig and Bloom, 1977; Blasse, 1994; van Eijk, 2002):

$$\eta_C(\lambda) = \frac{\bar{E}_\lambda}{\beta E_g} Sq = \frac{hc}{\bar{\lambda}} \frac{qS}{\beta E_g}, \tag{13a}$$

$$\bar{m}_O(E) = \eta_C(\lambda) \frac{E}{\bar{E}_\lambda} = \frac{E}{\beta E_g} Sq, \tag{13b}$$

where $\bar{E}_\lambda = hc/\bar{\lambda}$ is the mean energy of the emitted light photons, c is the light velocity, h is the Planck's constant, $\bar{\lambda}$ is the mean light wavelength, determined by the light spectrum measurements. E_g is the energy gap separating the valence and conduction energy bands (for ZnS, $E_g = 3.8$ eV) (Alig and Bloom, 1977). βE_g expresses the average energy required to create an electron–hole pair in the phosphor. This energy is larger than E_g. For ZnS it has been estimated that $\beta = 3$ (Blasse, 1994) and hence the corresponding energy is three times larger than the energy gap. S is the probability of energy transfer from the electron–hole pairs to the centers of light creation (luminescent centers) within the phosphor. q is the quantum efficiency of these centers, e.g. the efficiency to absorb energy and convert it into light photons. It has been previously estimated that for copper activated phosphors, the probability that electron–hole pairs are converted to light photons, Sq, is close to unity (Alig and Bloom, 1977; Blasse, 1994).

The light transmission efficiency of a phosphor layer, was expressed by the second integral in relations (1) and (4) in combination with (A.1) and (A.2) in Appendix A.

3. Results and discussion

Fig. 1 shows the absolute efficiency of four ZnS:Cu screens for various X-ray tube voltages in the mammographic energy range. Two separate curves are shown for the 20.15 mg/cm^2 screen corresponding to reflection and transmission mode of measurements. All the other curves were obtained in transmission mode. Points represent experimental data while the solid line is fitted curve calculated by Eqs. (2) and (1) of the theoretical absolute efficiency expression, as explained in Section 2.1. Fitting was performed following the Levenberg–Marquard method (Press et al., 1990), by allowing the value of optical attenuation parameters σ and β_0 to vary. The intrinsic conversion efficiency was assumed to be constant and equal to the value calculated by relation (13a) ($\eta_C = 0.23$, as shown later on). Best curve fitting was obtained for $\sigma = 41$ cm^2/g and $\beta_0 = 0.04$. For all screens absolute efficiency was found to increase continuously with increasing tube voltage. However, it is of interest to note the differences in the curve slopes, which are most prominent, between the 20.15 and 43.71 mg/cm^2 screens measured in transmission mode. In the very low tube voltage range from 22 to 26 kVp, the 20.15 mg/cm^2 screen was found to exhibit highest absolute efficiency values. For higher voltages up to 40 kVp, the 43.71 mg/cm^2 screen showed highest efficiency. Provided that the soft 22–26 kVp X-rays are equally absorbed within

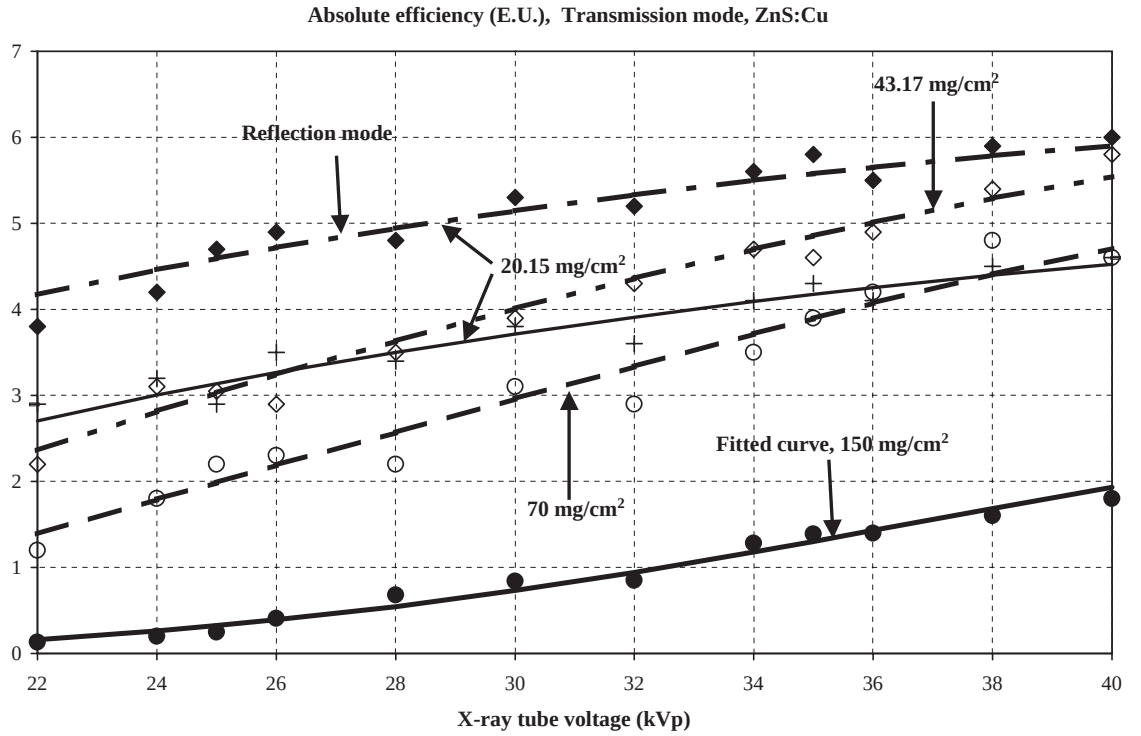

Fig. 1. Absolute efficiency of ZnS:Cu phosphor screens at various mammographic X-ray tube voltages (EU = efficiency unit: μW s/mR m^2).

all screens, the high efficiency of the 20.15 mg/cm^2 screen could be explained by considering that light attenuation effects are of lower importance within the thin screens. In addition, at 28 kVp, very often used in mammographic imaging techniques, the AE of 20.15 mg/cm^2 screen was found marginally lower than that of the 43.71 mg/cm^2 screen, which displays the highest AE. Thus the relatively high absolute efficiency of the thin (20.15 mg/cm^2) screen in the useful for mammography 25–28 kVp range, is a very interesting result, since thin screens show high-spatial resolution properties. As it is observed from the two curves of the 20.15 mg/cm^2 screen, reflection mode measurements exhibited higher efficiency values. This is so because most of the incident X-ray photons interact close to the irradiated screen surface. Hence, in comparison to transmission mode, light photons, produced at points of X-ray interaction, have to travel shorter distances to escape the X-ray-irradiated phosphor surface, thus suffering lower attenuation. The superiority of reflection over transmission mode AE values may provide a basis for comparison between conventional and digital mammography systems. Conventional mammography systems, regularly employing single-coated radiographic cassettes with reflection mode screen–film configuration, may show superior sensitivity than digital mammography detectors. However this comparison is only valid when the same screen thickness and phosphor material is used in both cases.

Fig. 2 shows a comparison between the ZnS:Cu absolute efficiency and three other ZnS-based phosphors, namely, the green light emitting ZnSCdS:Ag, ZnSCdS:Cu,Au phosphors and the bluish light emitting ZnS:Ag. Curves for ZnSCdS phosphors were traced from experimental data obtained in previous studies (Kandarakis et al., 1997, 2001a). The absolute efficiency of ZnS:Ag was calculated by relations (1) and(2) using data on η_C and σ determined as follows: η_C was calculated by relation (13a) using the same data as for ZnS:Cu except that the value of optical photon energy was $E_\lambda = 2.75$ eV, corresponding to $\lambda = 420$ nm (Alig and Bloom, 1977; Blasse, 1994). η_C was thus found to be 0.25. The value of σ for ZnS:Ag was determined by considering the variation of this coefficient with the mean value of the emitted light wavelength (Fig. 3). This variation was determined using data on σ and on emitted mean light wavelength, obtained from previous studies on various phosphors (Kandarakis et al., 1997; 2001a–c). It was found that σ varied according to the relation:

$$\sigma = a + b(\bar{\lambda})^{-1} + c(\bar{\lambda})^{-2}, \quad (15)$$

where a, b, c are fitted parameters. This variation of σ is in accordance with what was expected from the well-known light absorption and light-scattering laws, which state that light attenuation increases with decreasing wavelength (van de Hulst, 1957). Using relation (15) the value of σ for

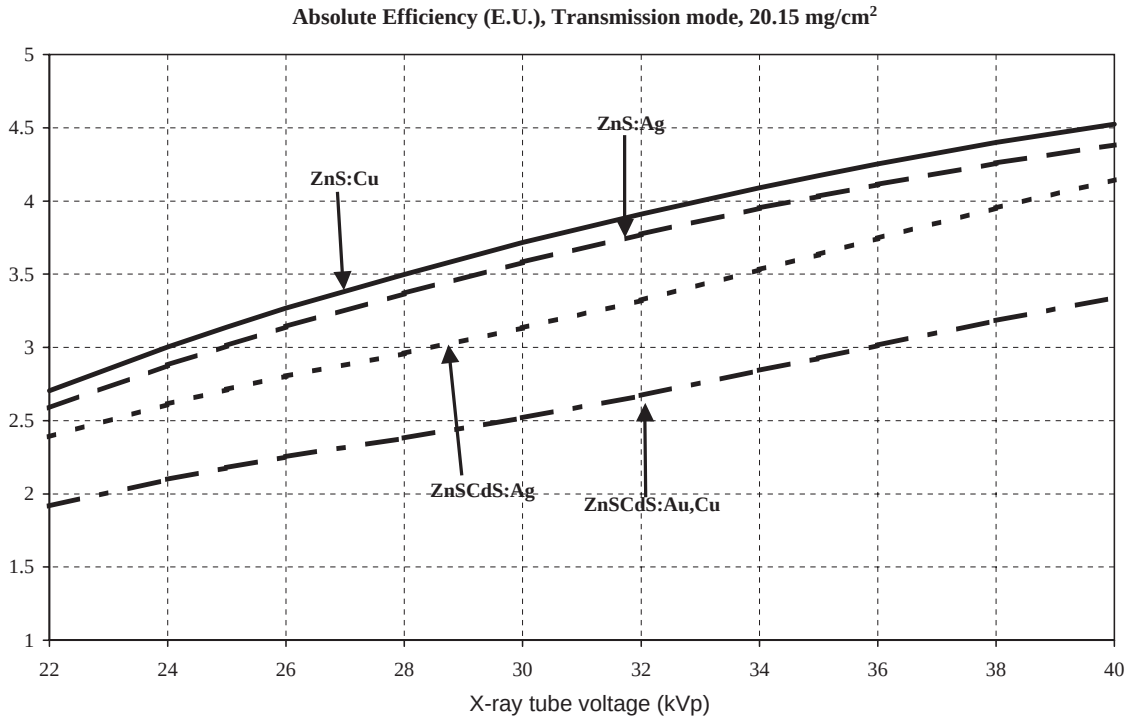

Fig. 2. Comparison of the absolute efficiency of ZnS:Cu, ZnS:Ag, ZnSCdS: Ag, ZnSCdS:Au,Cu phosphors at mammographic X-ray energies (EU = efficiency unit: $\mu W\,s/mR\,m^2$).

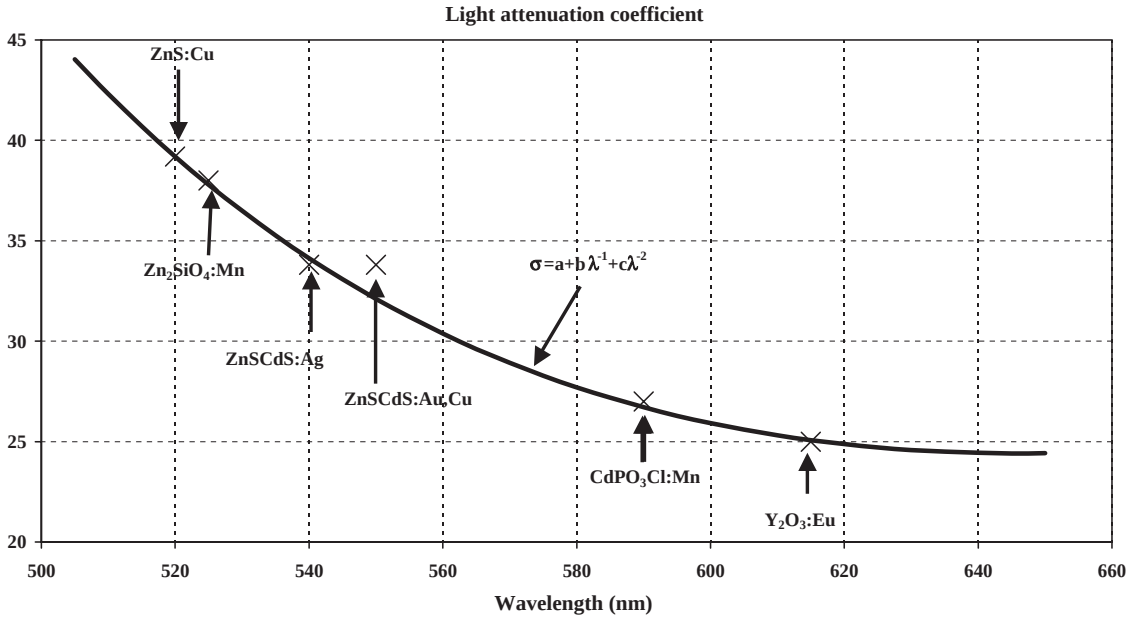

Fig. 3. Variation of the light attenuation coefficient (σ) values as a function of light wavelength corresponding to various phosphors (indicative data points displayed).

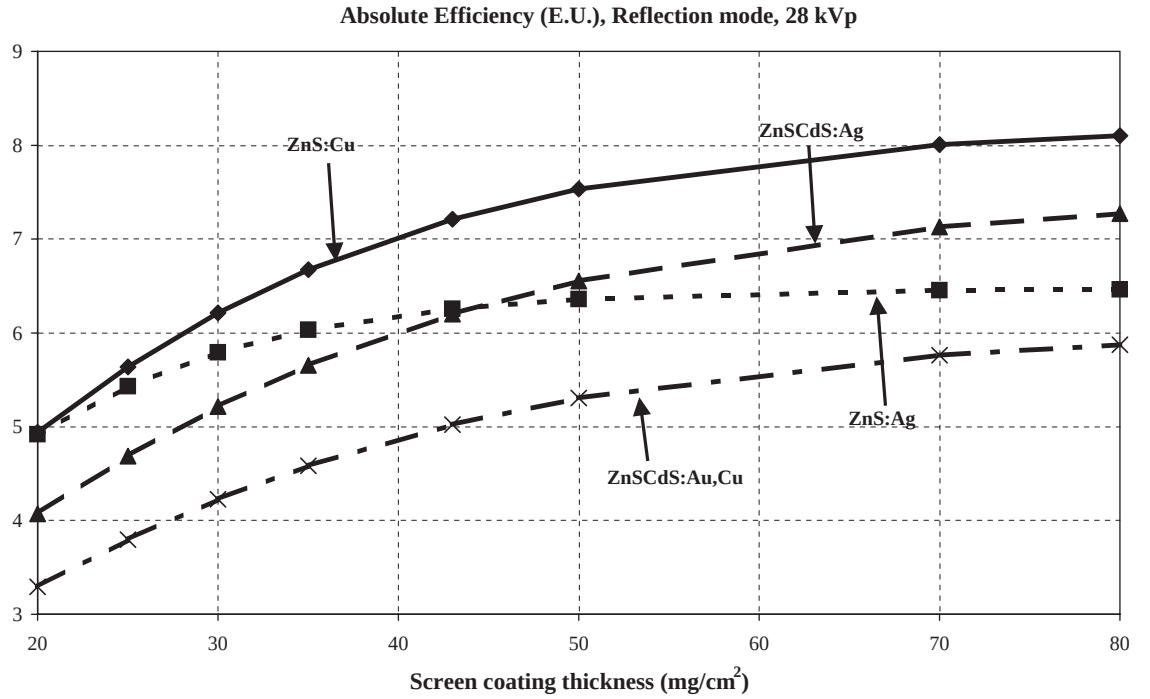

Fig. 4. Variation of the absolute efficiency with screen coating thickness, for ZnS:Cu, ZnS:Ag , ZnSCdS:Ag, ZnSCdS:Au,Cu phosphors, at 28 kVp (EU = efficiency unit: $\mu W\,s/mR\,m^2$).

ZnS:Ag was calculated to be $\sigma = 78\ cm^2/g$ given that $\lambda = 420$ nm. In a similar way β_0 was found equal 0.04. As it is observed from Fig. 2, ZnS:Cu shows higher AE than the other phosphors. Considering the two ZnS phosphors, they exhibit identical X-ray absorption and very similar light generation properties. Thus the higher efficiency of ZnS:Cu is due to the significantly lower value of its light attenuation coefficient σ. This is in accordance with what was expected from light scattering and light absorption laws (van de Hulst, 1957). Considering the ZnSCdS:Au,Cu and ZnSCdS:Ag phosphors, they were found with lower AE than ZnS:Cu due to their lower intrinsic conversion efficiency ($\eta_C = 0.17$ and 0.20, against $\eta_C = 0.23$ for ZnS:Cu) (Kandarakis et al., 1997, 2001a). This result is important for ZnS:Cu, since it implies lower X-ray patient dose burden, compared to the other two phosphors, for a given level of image brightness.

In Fig. 4 the absolute efficiency of the four phosphors is shown for screens of various coating thicknesses, measured at 28 kVp in reflection mode of measurements. Absolute efficiency was found to increase continuously with increasing thickness showing a tendency to saturate at a value slightly higher than $\eta_A = 8\ \mu W m^{-2} R^{-1}$ s. It should be noted however that, in transmission mode measurements, not shown in figure, absolute efficiency showed a maximum for the 43.71 mg/cm^2 screen and a net decrease for thicker screens (see also Fig. 1).

Fig. 5 shows the Monte-Carlo simulation results for X-ray photon interactions within a 43.71 mg/cm^2 ZnS phosphor screen. Shown are (i) the fraction of incident X-ray energy flux absorbed (total absorbed), (ii) the fraction of energy flux absorbed following photon scattering (scatter and absorbed), and (iii) the fraction of energy flux transmitted (transmitted) through the screen. Scatter and absorbed fraction is presented in the secondary axis (right vertical axis) of Fig. 5. Scattering is a factor contributing to image resolution degradation, while the transmitted flux fraction represents X-ray energy losses causing absolute efficiency deterioration. As it may be observed the absorption efficiency (total absorbed) of ZnS maintains high values in the useful for mammography energy range between 15 and 30 keV. For higher energies total X-ray absorption decreases more rapidly. In the 15–30 keV energy range the behavior of the phosphor is dominated by photoelectric absorption. This is reinforced by the fact that within the 15–30 keV energy range the scatter and absorbed fractions are very low (below 4.5%).

Shown in Fig. 6 are the MTF curves of various ZnS:Cu screens measured at 28 kVp in reflection mode. The screen of 20.15 mg/cm^2 (also shown in transmission mode) was found to exhibit by far the highest MTF values in the whole frequency range, e.g. about 0.9 at 20 lp/cm, 0.6 at 50 lp/cm and maintained a value higher than 0.3 at 100 lp/cm. The MTF of the 43.71 mg/cm^2 screen was found

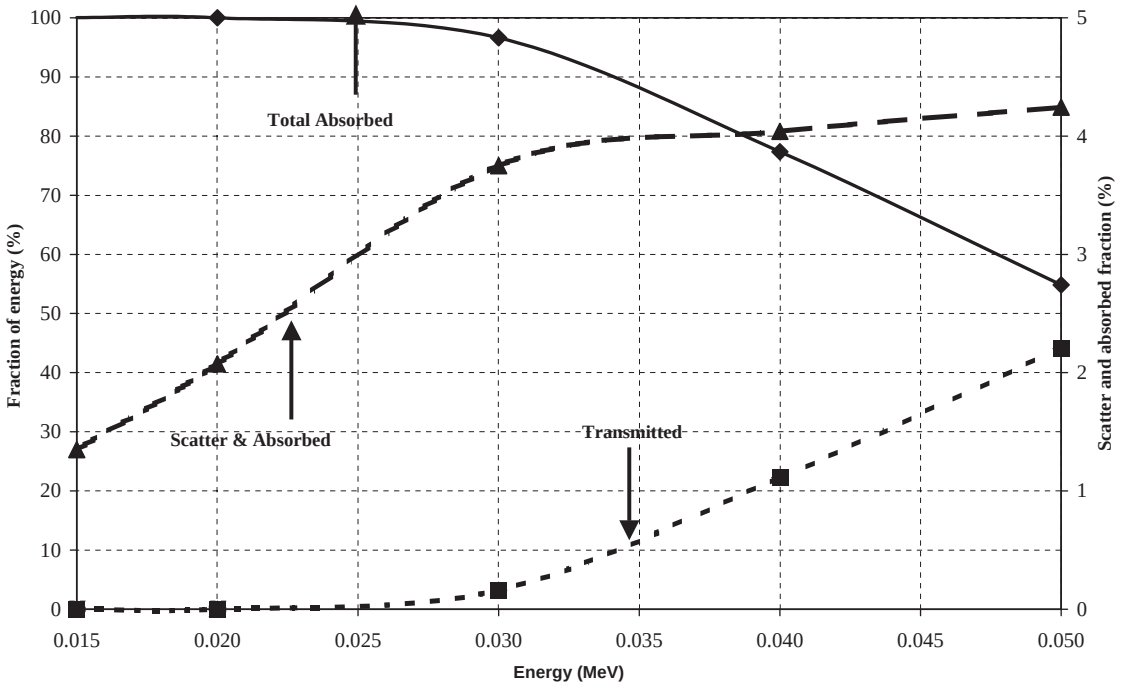

Fig. 5. Monte-Carlo simulation results representing X-ray photon interactions (X-ray absorption, scattering and transmission) within the 43.71 mg/cm^2 ZnS phosphor screen.

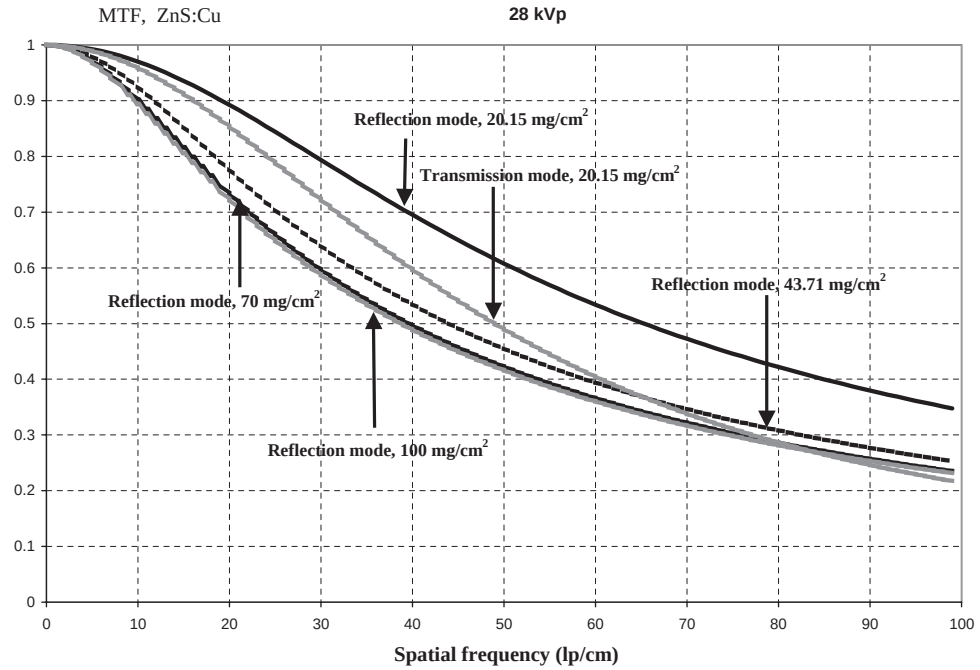

Fig. 6. Modulation transfer function (MTF) of various ZnS:Cu screens determined at 28 kVp.

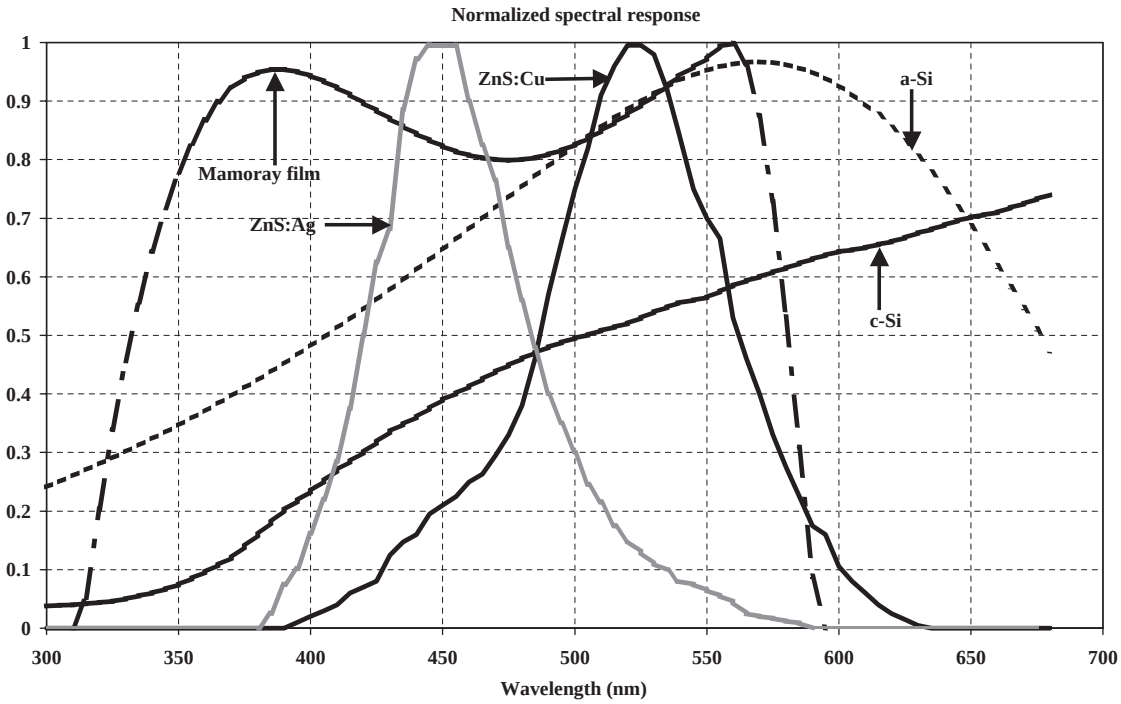

Fig. 7. Normalized emission spectra of ZnS:Ag and ZnS:Cu phosphors and spectral sensitivity curves of a-Si, c-Si photodiodes and mamoray film.

approximately 30% lower than that of 20.15 mg/cm^2 screen, in the medium and high spatial frequency range, while the MTF curves of the 70 and 100 mg/cm^2 screens were found very close to each other. MTF curves, not shown in figure, of similar shape were obtained in transmission mode measurements, however corresponding to significantly lower values (e.g. 0.6 at 50 lp/cm instead of 0.7 in reflection mode for the 20.15 mg/cm^2). According to these results and taking into account the absolute efficiency data in the 25–28 kVp voltage range, the 20.15 mg/cm^2 screen may provide the optimal combination of efficiency and spatial resolution for mammographic imaging. The superiority of reflection over transmission mode MTF values demonstrates the superior resolution properties of conventional over digital mammography detectors for identical phosphor material and equal phosphor thickness.

Fig. 7 shows the measured light emission spectrum of the ZnS:Cu phosphor, together with the ZnS:Ag spectrum taken from the literature (Knoll, 1989). Spectral sensitivity curves of various photodetectors are also shown. As it may be observed the light spectrum of ZnS:Cu is situated well within the limits of the spectral sensitivity curve corresponding to the amorphous silicon (a-Si) photodetector. In addition, the peak value of the light spectrum found at 520 nm is very close to the a-Si sensitivity maximum at 560–570 nm. This is interesting since a-Si is used in photodetectors of modern digital radiography flat-panel imagers. The ZnS:Cu spectrum is also within the limits of the crystalline-silicon (c-Si) and the ortho-chromatic (Agfa mamoray) film spectral sensitivities. ZnS:Cu may thus be efficiently combined with photodetectors (including CCD) used in both conventional and digital radiography. Compared to ZnS:Cu, the position of ZnS:Ag light spectrum corresponds to lower a-Si and c-Si sensitivity values resulting in lower spectral compatibility. Table 1 shows the values of the spectral compatibility factors calculated according to relation (3). The values corresponding to ZnS:Cu were found adequately high, especially those corresponding to a-Si (0.86) and to film (0.834). Using wavelength data from Fig. 7 ($\lambda = 520$ nm for ZnS:Cu), the ZnS:Cu intrinsic efficiency for conversion of absorbed X-rays into light photons was calculated by relation (13a) and it was found equal to 0.23.

Table 1
Spectral compatibility factors

Phosphors	Amorphous silicon	Crystalline silicon	Mamoray film
ZnS:Cu	0.859	0.518	0.834
ZnS:Ag	0.693	0.413	0.838
ZnSCdS:Au,Cu	0.900	0.577	0.500
ZnSCdS:Ag	0.842	0.572	0.571

Fig. 8 shows DQE curves of various screens determined at 28 kVp in reflection mode. Transmission mode DQE

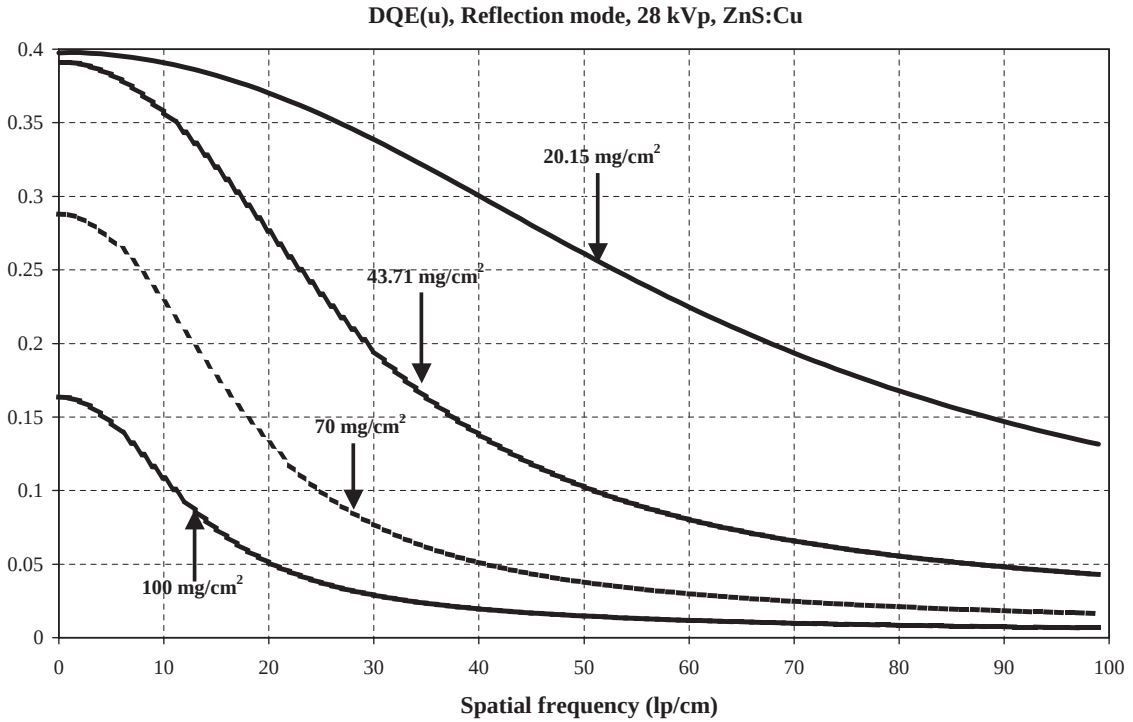

Fig. 8. Frequency dependent detective quantum efficiency (DQE) of various ZnS:Cu screens determined at 28 kVp.

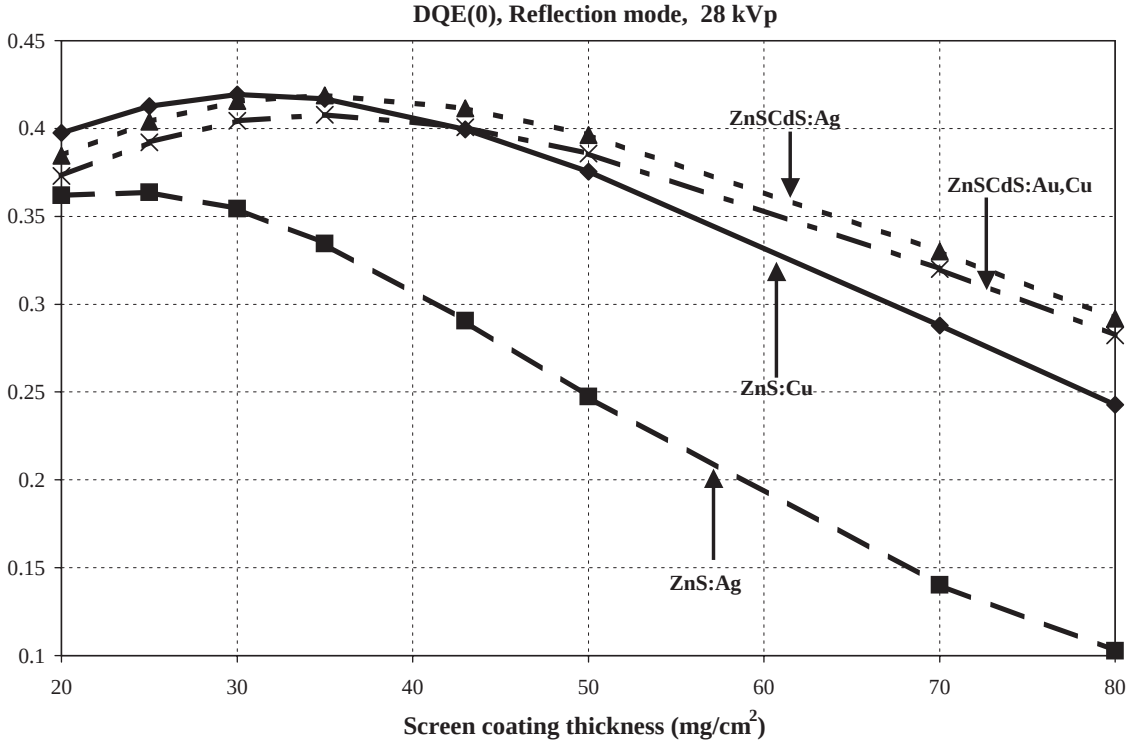

Fig. 9. Variation of calculated zero-frequency detective quantum efficiency with screen coating thickness for ZnS:Cu, ZnS:Ag, ZnSCdS:Ag, ZnSCdS:Au,Cu at 28 kVp.

values, not shown in figure, were slightly lower. Maximum DQE was found for the screen of 20.15 mg/cm^2. In the whole frequency range up to 100 lp/mm, this screen maintained relatively high values ranging from 0.4 at zero frequency, down to 0.13 at 100 lp/cm. As it is observed DQE decreased rapidly with frequency and screen thickness. For thick screens (100 mg/cm^2) DQE was found considerably lower than 0.2, at zero frequency, and lower than 0.1 for frequencies higher than 15 lp/cm. These results indicate that DQE is principally affected by the corresponding MTF behavior (see also Fig. 6). It is also of importance to note the high DQE performance of the 20.15 mg/cm^2 screen, which was also found to exhibit high AE and maximum MTF.

Fig. 9 illustrates the variation of calculated DQE, at zero frequency, with screen thickness for ZnS:Cu, ZnS:Ag, ZnSCdS:Ag, ZnSCdS:Cu,Au phosphors. DQE of ZnS:Cu was found higher than that of the other phosphors in the range from 20 to approximately 35 mg/cm^2. For thicker screens ZnSCdS:Ag exhibited highest DQE. DQE data demonstrate that DQE values of ZnS:Cu screens are high enough for application in radiographic imaging. This may be understood if a comparison is made with published experimental DQE data, obtained on commercial radiographic screens (Dick and Motz, 1981). It is also of significance to note that DQE was found highest for screens in the range between 20 and 45 mg/cm^2, which is often used in X-ray mammography. ZnS:Cu showed clearly higher DQE values than ZnS:Ag.

In conclusion ZnS:Cu is a high intrinsic conversion efficiency phosphor emitting a light spectrum which is adequately compatible with the sensitivities of amorphous silicon photodiodes and ortho-chromatic films. Taking into account (i) its absorption efficiency at low X-ray energies and (ii) its light emission and image quality properties, this phosphor could be considered for use in mammographic detectors, both radiographic cassettes and digital imagers, provided that fast decay characteristics are not necessary.

Acknowledgements

This study is dedicated to the memory of Prof. G.E. Giakoumakis, leading member of our team, whose work on phosphor materials has inspired us to continue.

Appendix A

1. The function ψ in relation (1) was expressed as

$$\bar{\psi}(E,w)=\frac{\mu(E)\exp[-\mu(E)w]\,\mathrm{d}w}{\int_0^{w_O}\mu(E)\exp[-\mu(E)w]\,\mathrm{d}w}, \tag{A.1}$$

where $\mu(E)$ is the total mass energy absorption coefficient of the phosphor material. The numerator gives the probability for an X-ray photon to be absorbed at depth w within the phosphor and the denominator gives the total probability of X-ray absorption within the whole phosphor.

2. The function g_λ, giving the fraction of light escaping to the output per X-ray absorbed, was expressed by the formula (Ludwig, 1971; Swank, 1973):

$$\bar{g}_\lambda(\sigma,w)=\frac{\rho_1[(\beta_0+\rho_0)\mathrm{e}^{\sigma w}+(\beta_0-\rho_0)\mathrm{e}^{-\sigma w}]}{(\beta_0+\rho_0)(\beta_0+\rho_1)\mathrm{e}^{\sigma w_0}-(\beta_0-\rho_0)(\beta_0-\rho_1)\mathrm{e}^{-\sigma w_0}}, \tag{A.2}$$

where σ is a light attenuation coefficient of the phosphor (Hamaker, 1947; Ludwig, 1971), also defined as the reciprocal of the light photon diffusion length (Swank, 1973). σ has been expressed as a function of the optical scattering coefficient (s) and the optical absorption coefficient (a):

$$\sigma=[a(a+2s)]^{1/2}. \tag{A.3a}$$

According Swank (1973) σ may be expressed in the Fourier domain, as a function of spatial frequency (u):

$$\sigma(u)=[\sigma^2+4(\pi u/d)^2]^{1/2}, \tag{A.3b}$$

where d is the density of the phosphor material. Hence the emitted light photon flux (Φ_λ in relations (4)–(6)) may be also expressed in the Fourier domain, as a function of spatial frequency.

ρ_0, ρ_1 are light reflectivity parameters expressing the reflection of light at the front and back phosphor surfaces defined as

$$\rho_n=(1-r_n)/(1+r_n), \quad n=0,1, \tag{A.4}$$

where r_n denotes the optical reflection coefficients at the front (0) and back (1) screen surfaces.

β_0 is a light reflectivity parameter, like ρ, corresponding to a very thick phosphor screen with no light transmission through it. β_0 has been also expressed as a function of optical absorption and optical scattering coefficients (Hamaker, 1947; Ludwig, 1971):

$$\beta_0=[a/(a+2s)]^{1/2}. \tag{A.5}$$

Absolute efficiency (relation (2)) was then calculated as follows: ρ_n were assumed to be equal to those obtained in previous studies ($\rho_0=1$ and $\rho_1=0.89$) described by Ludwig (1971). η_C was calculated by relation (13a). These data were then used in order to fit relation (2) to the experimental absolute efficiency curves. Using the Levenberg–Marquardt method (Press et al., 1990), best fit was obtained, for specific values of the parameters σ and β_0 (41 cm^2/g and 0.04, respectively). These values, together with η_C and ρ_n, were then adopted as the intrinsic optical properties of the phosphor.

References

Alig, R.C., Bloom, S., 1977. Cathodoluminescent efficiency. J. Electrochem. Soc. 124, 1136–1138.

Barnes, G.T., 1979. The use of bar pattern test objects in assessing the resolution of screen/film systems. In: Haus, A.G. (Ed.), The Physics of Medical Imaging: Recording System Measurements and Techniques. American Association of Physicists in Medicine, New York, pp. 138–151.

Blasse, G., 1994. The luminescence efficiency of scintillators for several applications: state-of-the-art. J. Luminescence 60 & 61, 930–935.

Boone, J.M., Seibert, J.A., Sabol, J.M., Tecotzky, M., 1999. A Monte-Carlo study of X-ray fluorescence in X-ray detectors. Med. Phys. 26, 905–916.

Chan, H.P., Doi, K., 1983. The validity of Monte-Carlo simulation in studies of scattered radiation in diagnostic radiology. Phys. Med. Biol. 28, 109–129.

Dick, C.E., Motz, J.W., 1981. Image information transfer properties of X-ray fluorescent screens. Med. Phys. 8, 337–346.

Greening, J.R., 1985. Fundamentals of Radiation Dosimetry. Institute of Physics, London, p. 56.

Hamaker, H., 1947. Radiation and heat conduction in light-scattering materials. Philips Res. Rep. 2, 55.

Hell, E., Knüpfer, W., Mattern, D., 2000. The evolution of scintillating medical detectors. Nucl. Instrum. Meth. Phys. Res. A 454, 40–48.

Hubbell, J.H., Overbo, I., 1979. Relativistic atomic form factors and photon coherent scattering cross sections. J. Phys. Ref. Data 18, 69–105.

Hubbell, J.H., Seltzer, S.M., 1995. Tables of X-ray mass attenuation coefficients and mass energy absorption coefficients 1 keV to 20 MeV for elements $Z = 1$ to 92 and 48 additional substances of dosimetric interest. US Department of Commerce. NISTIR 5632.

Hubbell, J.H., Veigele, W.J., Briggs, E.A., Brown, R.T., Cromer, D.T., Howereton, R.J., 1975. Atomic form factors, incoherent scattering functions and photon scattering cross sections. J. Phys. Ref. Data 4, 471–495.

Hubbell, J.H., Trehan, P.N., Singh, N., Chand, B., Mehta, D., Garg, M.L., Garg, R.R., Singh, S., Puri, S., 1994. A review, bibliography, and tabulation of K, L, and higher atomic shell X-ray fluorescence yields. J. Phys. Chem. Ref. Data 23, 339–364.

ICRU (International Commission on Radiological Units), 1986. Modulation transfer functions of screen–film systems. ICRU Report 41.

Kandarakis, I., Cavouras, D., Panayiotakis, G., Nomicos, C., 1997. Evaluating X-ray detectors for radiographic applications: a comparison of ZnSCdS:Ag with Gd_2O_2S:Tb and Y_2O_2S:Tb screens. Phys. Med. Biol. 42, 1351–1373.

Kandarakis, I., Cavouras, D., Nomicos, C.D., Panayiotakis, G.S., 2001a. X-ray luminescence of ZnSCdS:Au, Cu phosphor using X-ray beams for medical applications. Nucl. Instrum. Meth. Phys. Res. B 179, 215–224.

Kandarakis, I., Cavouras, D., Nomicos, C.D., Panayiotakis, G.S., 2001b. Measurement of the X-ray luminescence and spectral compatibility of the $CdPO_3Cl$:Mn phosphor. Radiat. Meas. 33, 217–224.

Kandarakis, I., Cavouras, D., Panayiotakis, G.S., Nomicos, C.D., 2001c. Experimental investigation of the optical signal, gain, signal to noise ratio and information content characteristics of X-ray phosphor screens. Appl. Phys. B 72, 877–883.

Knoll, G.N., 1989. Radiation Detection and Measurement. Wiley, New York, 237pp.

Ludwig, G.W., 1971. X-ray efficiency of powder phosphors. J. Electrochem. Soc. 118, 1152–1159.

Press, W.H., Flannery, B.P., Teukolsky, S.A., Vetterling, W.T., 1990. Numerical recipes in C: the art of scientific computing. Cambridge University Press, Cambridge, pp. 540–547.

Shaw, R., Van Metter, R., 1984. An analysis of the fundamental limitations of screen–film systems for X-ray detection. Proc. SPIE 454, 128–132.

Storm, E., Israel, H., 1967. Photon cross-sections from 0.001 to 100 MeV for elements 1 through 100 Report LA-3753 Los Alamos Scientific Laboratory of the University of California

Swank, R., 1973. Calculation of modulation transfer functions of X-ray fluorescent screens. Appl. Opt. 8, 1865–1870.

Tucker, D.M., Barnes, G.T., Wu, X., 1991. Molybdenum target X-ray spectra: a semi-empirical model. Med. Phys. 18, 402–407.

van de Hulst, H.C., 1957. Light Scattering by Small Particles. Wiley, New York, pp. 103–107.

van Eijk, C.W.E., 2002. Inorganic scintillators in medical imaging. Phys. Med. Biol. 47, R85–R106.

Wieczorek, H., 2001. Physical aspects of detector design. Radiat. Meas. 33, 541–545.

Williams, M.B., Simoni, P.U., Smilowitz, L., Stanton, M., Phillips, W., Stewart, A., 1999. Analysis of the detective quantum efficiency of a developmental detector for digital mammography. Med. Phys. 26, 2273–2285.